

Optimizing signal recycling for detecting a stochastic gravitational-wave background

Duo Tao*

Physics and Astronomy, Carleton College, Northfield, MN 55057, USA

Nelson Christensen†

*Physics and Astronomy, Carleton College, Northfield, MN 55057, USA and
ARTEMIS, Université Côte d’Azur, Observatoire Côte d’Azur,
CNRS, CS 34229, F-06304 Nice Cedex 4, France*

(Dated: December 14, 2024)

Signal recycling is applied in laser interferometers such as the Advanced Laser Interferometer Gravitational-Wave Observatory (aLIGO) to increase their sensitivity to gravitational waves. In this study, signal recycling configurations for detecting a stochastic gravitational wave background are optimized based on aLIGO parameters. Optimal transmission of the signal recycling mirror (SRM) and detuning phase of the signal recycling cavity (SRC) under a fixed laser power and low-frequency cutoff are calculated. Based on the optimal configurations, the compatibility with a binary neutron star (BNS) search is discussed. Then, different laser powers and low-frequency cutoffs are considered. Two models for the dimensionless energy density of gravitational waves $\Omega_{gw}(f) = \Omega_\alpha(f/f_{ref})^\alpha$, the flat model $\alpha = 0$ and the $\alpha = 2/3$ model, are studied. For a stochastic background search, it is found that an interferometer using signal recycling has a better sensitivity than an interferometer not using it. The optimal stochastic search configurations are typically found when both the SRM transmission and the SRC detuning phase are low. In this region, the BNS range mostly lies between 160 and 180 Mpc. When a lower laser power is used (reducing radiation pressure at low frequencies), the optimal SRC detuning phase increases, the optimal SRM transmission increases and the optimal sensitivity improves. A reduced low-frequency cutoff gives a better sensitivity limit. For both models of Ω_{gw} , a typical optimal sensitivity limit on the order of 10^{-10} is achieved at a reference frequency of $f_{ref} = 25$ Hz.

I. INTRODUCTION

The search for a stochastic gravitational wave background (SGWB) has been important in our understanding of the universe, even if the SGWB has yet to be detected [1–5]. The Advanced Laser Interferometer Gravitational-Wave Observatory (aLIGO), one of the most sensitive scientific instruments in the world, has been shown to be sensitive enough to detect gravitational waves in its first and second observation runs [6–12]. Advanced Virgo [13], observing in the second observing run with aLIGO also participated in two detections [11, 12]. In the coming observation runs, it is expected that more about the SGWB will be understood as the detectors’ sensitivities improve and the LIGO-Virgo network can make deeper searches [14, 15].

The introduction of the signal recycling system in aLIGO improves the sensitivity of the interferometers [16]. In this paper, we will show that an interferometer system with signal recycling is more sensitive for detecting the SGWB than a system without. Also, we derive the optimal configurations of the signal recycling mirror (SRM) that could achieve an optimal sensitivity for detecting a SGWB with a dimensionless energy density $\Omega_{gw}(f)$ on the order of 10^{-10} .

Section II presents the general approach to optimize

the SGWB search and the result for a particular power usage and frequency cutoff. Section III considers the optimization under a different laser power and low-frequency cutoff. Section IV considers the $\Omega_{gw}(f) \propto f^{2/3}$ power-law model [14] for the SGWB. Section V summarizes the results of this project and considers possible topics of future work.

II. OPTIMIZATION FOR THE SGWB SEARCH

A. Parameters of the SRM

The aLIGO optical configuration is displayed in Fig. 1 [16]. The SRM is a mirror at the output port of the interferometer, sending part of the signal back into the interferometer to create resonances at certain frequencies in order to amplify the signal sensitivity [17, 18].

We are interested in two parameters of the SRM, the transmission and the signal recycling cavity (SRC) detuning phase. It should be noted that the transmission is the power transmission, the percentage of power transmitted through the mirror, in contrast to the amplitude transmission. It is given as [19]

$$T = 1 - R - \lambda_{SR} \quad (1)$$

where R is the reflectivity, T is the transmission and λ_{SR} is the loss inside the SRC, which is the sum of mismatch loss and beamsplitter loss. In this work, we assume that the mismatch loss is zero and the beamsplitter loss is

* taod@carleton.edu

† nelson.christensen@oca.eu

TABLE I: Parameters for the four configurations involved in the comparison. The BNS ranges and the Ω_{gw} are calculated assuming an input laser power of 125 W and low-frequency cutoff 10 Hz.

Configuration	SRM transmission	SRC detuning phase (degree)	Ω_{gw}	BNS Range(Mpc)
No recycling	1	0	1.08×10^{-8}	116.55
Optimal BNS	0.2	16	2.28×10^{-9}	207.94
Optimal SGWB	0.015	2.7	6.84×10^{-10}	154.41
Nominal	0.33	0	2.31×10^{-9}	191.17

of the optimization results. However, computational resources limit the size of the steps such that if the steps are too small, there will be too many candidate configurations produced and the amount of computations would be unfeasible. Therefore, we take the following two-step approach to obtain a finer optimization without too much computational burden.

1. We start with a full scan over the whole region with transmission resolution of 0.1% and phase resolution of 1° . Transmission ranges from 0% to 100% and the phase ranges from -180° to 180° . Therefore, there will be $1000 \times 180 = 180000$ configurations considered and the accuracy of the results is 0.1% and 1° .
2. Then, we do a localized scan within the accuracy limit around the optimization configurations we get in the first step. Suppose in the first step we find transmission T and phase ϕ achieve the best sensitivity. We then scan the 2D domain $[T - 0.1\%, T + 0.1\%] \times [\phi - 1^\circ, \phi + 1^\circ]$ with a transmission resolution of 0.01% and a phase resolution of 0.1° , both ten times finer than the first step. Thus, the second step involves $20 \times 20 = 400$ configurations in total.

Hence, the method above gives results with accuracy of 0.01% in transmission and 0.1° in phase.

However, this method has its shortcomings such that in the second step we might be approximating a local optimum. If there are multiple local optima and in the first step we locate a local optimum that is not the global optimum due to insufficient resolution, the second step will only get us closer to the local optimum. The problem of insufficient resolution always exists when we optimize a function numerically. However, we shall explain at the end of this section that this might not be a significant problem for this work.

D. Optimization results

We assume 125 W incident on the power recycling mirror. Using the method described above, it is found that 1.5% transmission and 2.7° of detuning phase give us the optimal SGWB sensitivity with the limit of Ω_0 being 6.84×10^{-10} . The optimal noise spectrum is shown in Fig. 3. We can see a dip at the low frequency range

around 25 Hz, which should explain why this configuration does well for SGWB search. The f^{-6} term in Eq. 6 gives the low frequency noise spectrum much more weight than the high frequency part so a low frequency improvement is more effective to enhance the SGWB sensitivity.

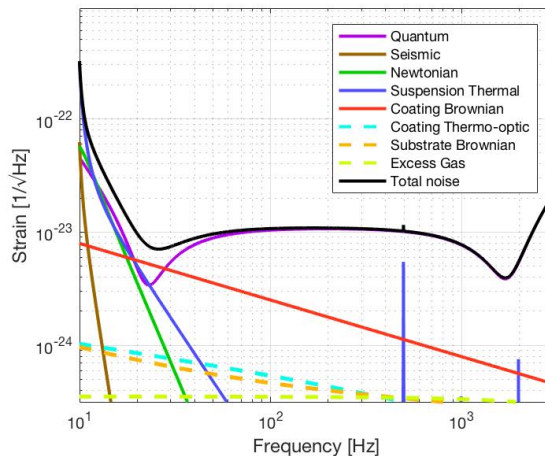


FIG. 3: The noise spectrum for the optimal SGWB configuration at 125W, with the low-frequency cutoff as 10Hz. The detuning phase is 2.7° and the transmission is 1.5% [23].

E. Comparison with other configurations

The total noise spectrum of a SGWB optimized configuration is compared with other configurations in Fig. 2. There are three other configurations with which we have interest: no signal recycling, the configuration optimized for a binary neutron star (BNS) search and the nominal configuration.

1. **No signal recycling:** when there is no signal recycling installed in the interferometer, all light passes so we set the transmission to one, and the Gouy phase does not exist so it is zero. Its total noise spectrum is shown on the left of Fig. 2, compared with the optimal SGWB configuration. The sensitivity limit for this is 1.08×10^{-8} .
2. **Optimal BNS search:** this configuration (transmission 20% and detuning phase 16°) has optimal BNS range of $210Mpc$ [16]. Its spectra is shown in

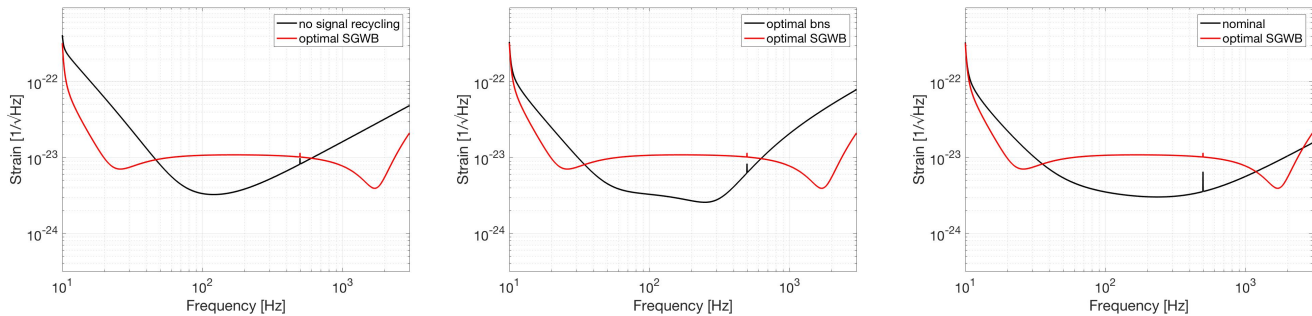


FIG. 2: Comparison of the noise spectra optimized for a SGWB search with other configurations. On the left, middle, right are no signal recycling (transmission = 1, phase = 0), BNS optimized (transmission = 20%, phase = 16°) and nominal configurations (transmission = 33% and phase = 0), respectively.

in the middle of Fig. 2. We can see that its optimization is different than the optimal SGWB spectra in Fig. 3. The former has its best sensitivity around mid-frequency 100 Hz while the latter benefits the most from low-frequency improvements.

3. Nominal configuration: the nominal configuration (transmission 33% and phase zero) has a flat and smooth noise spectrum shown on the right of Fig. 2.

From all of the three comparison plots of in Fig. 2, it can be seen that the optimal SGWB configuration has a significant improvement at low frequencies. At the same time, there is a sacrifice of mid-frequency performance around 100 Hz. However, since the low-frequency sensitivity is more important for a SGWB search, it still has the best sensitivity.

Parameters for the optimal SGWB search and the other three configurations are summarized on Table I. The SGWB optimized configuration is about three times more sensitive than the BNS optimized configuration for SGWB search. Also, the BNS optimized configuration has a BNS range 53 Mpc further than the BNS range of the SGWB configuration. If we were to choose one configuration to use for both the SGWB search and the BNS search among the four configurations in Table I, the BNS optimized configuration would probably be the choice since it has the best BNS range and a reasonable SGWB $\Omega_{gw}(f)$ limit.

F. Compatibility with BNS search

In this section, we will address the question as to whether there is a particular signal recycling configuration such that a SGWB search could be compatible with a BNS search. There are two approaches used here.

The first approach is quantitative. We are looking for a configuration that has good sensitivities for both the SGWB search and the BNS search. Based on this, we can limit the scope to configurations having nominally

good sensitivities for the SGWB search. Thus, we list all configurations that give $\Omega_{gw} < 10^{-9}$ and calculate the maximum BNS range among them. It is found that the maximum BNS range is 165 Mpc. Compared with the 210 Mpc for the BNS optimized configuration and 191 Mpc for the nominal configuration, these configurations are significantly less effective for a BNS search.

The second approach is qualitative. We plot all Ω_{gw} and BNS ranges on a 2D region of the $[transmission \times detuningphase]$ space. The plots are shown in Fig. 4. Both the SGWB search and the BNS search are optimized on the center of the left edge where the phase and transmission are low. However, the darkest region of the SGWB plot is even closer to the origin than the optimal (brightest) region of the BNS range. The optimal configuration of the SGWB search has even lower transmission and phase. It also deteriorates more quickly as the transmission and phase increases. When it gets close to the high BNS range region, the sensitivity rapidly worsens.

Also, with the information in Fig. 4, we are now able to address the issue left in part C. In part C, we were worried about the validity of our method such that there might be a global optimal configuration between the smallest steps of our scanning of the phase and transmission. However, examining the colors in Fig. 4, we notice that there is not another region that has Ω_{gw} comparable to the darkest region around the origin. Thus, since we located the optimum in the low-phase and low-transmission region, $1.5\% \pm 0.01\%$ transmission and $2.7 \pm 0.1^\circ$ detuning phase, it is unlikely for other local optima to compete with it.

III. USING A DIFFERENT LASER POWER AND LOW-FREQUENCY CUTOFF

For all the work above, we have assumed a laser power of 125 W and low-frequency cutoff of 10 Hz. In this section, we will optimize the signal recycling parameters using different laser powers and low-frequency cutoffs, while keeping all of the other aLIGO (target sensitivity) noise terms the same.

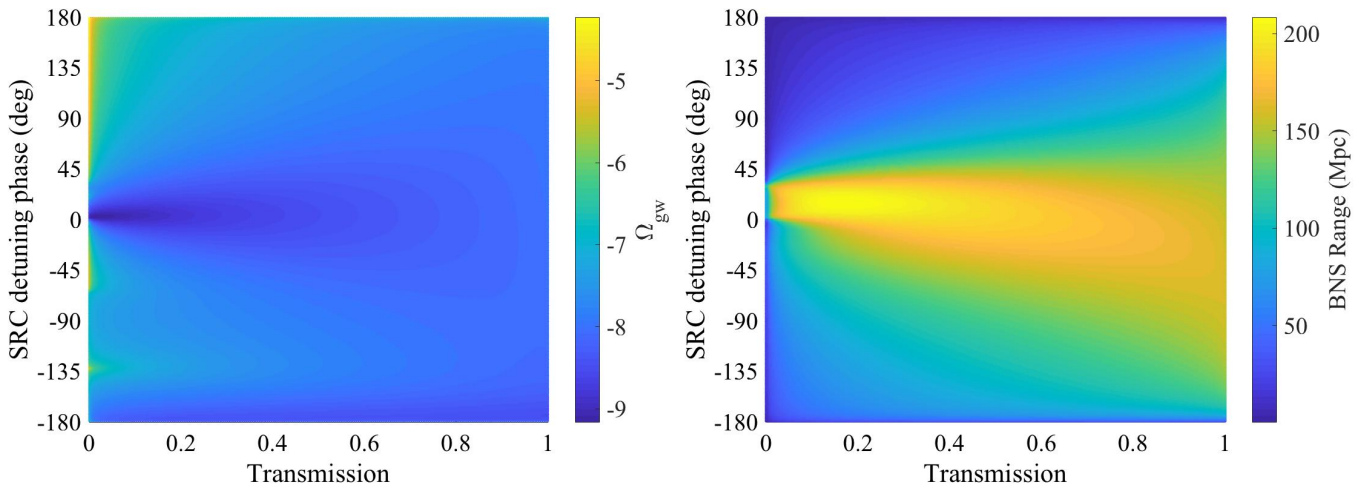


FIG. 4: Plots of Ω_{gw} and the BNS range as functions of SRM transmission and SRC detuning phase, assuming a laser power input of 125 W and low-frequency cutoff of 10 Hz.. On the left is Ω_{gw} plotted on log (10) scale. On the right is the BNS range. We can see that both of them are optimized in the low-phase low-transmission region close to the origin. However, the optimal region for Ω_{gw} is smaller and closer to the origin than the optimal region of the BNS range.

A. Optimal configurations

The relation between power and the optimization is investigated in two groups: low power below 5 W and high power above 5 W up to 200 W. For the high power, all interferometers with laser powers from 5 W to 200 W, in steps of 5 W, are optimized. For the low power, we optimize all interferometers with laser powers from 0.5 W up to 5 W in steps of 0.5 W. Different low-frequency cutoffs, 10 Hz, 15 Hz and 20 Hz, are also considered. Therefore, combining 49 laser powers with 3 low-frequency cutoffs for each power, the signal recycling of 147 possible interferometer parameters are optimized. The optimal configurations are plotted in Fig. 5.

From Fig. 5, we find that for high laser power input both the optimal transmission and the optimal phase decrease when we increase the power input. From 5 W to 200 W with a 10 Hz cutoff, the optimal transmission decreases from 19.8% to 1.0% and the optimal phase decreases from 60° to 1.7° . This means that the optimum configuration will move to the bottom left in Fig. 4 if we increase the laser power. Also, the low-frequency cutoff does not significantly change the optimal signal recycling configurations, with the three lines being close in Fig. 5. In the meanwhile, for low laser power input below 5 W, the optimal transmission peaks at about 2 W and decreases quickly under 2 W. The optimal detuning phase follows the same pattern as high power and keeps increasing up to 120° at 0.5 W with 10 Hz cutoff.

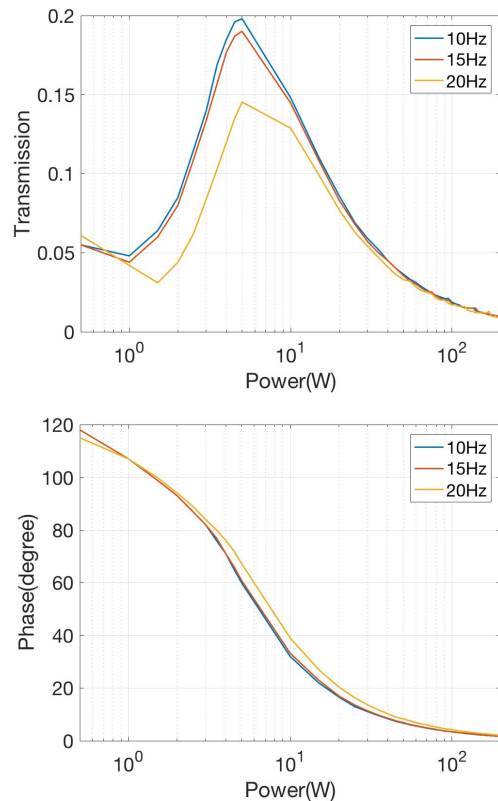


FIG. 5: Optimal SRC configurations as a function of input laser power. The top plot shows the relation between the optimal SRM transmission and power. The optimal transmission peaks around 2 W and then decreases above that. The bottom plot displays the decrease of optimal SRC detuning phase with laser power.

B. Optimal Ω_{gw}

The relation between laser power, low-frequency cutoff and the optimal sensitivity Ω_{gw} is presented in Fig. 6. These correspond to the optimal configurations found in Fig. 5. As the power decreases, the sensitivity improves and is the best around 1.5 W. The optimal powers are 1.5 W for 10 Hz and 15 Hz cutoff, and 2 W for 20 Hz cutoff. For 10 Hz cutoff and 1.5 W laser power, the optimal Ω_{gw} is 5.7×10^{-10} , which is the global optimal sensitivity among all interferometer configurations considered. When the laser power is above 5 W, the sensitivity gets worse as the laser power increases. Assuming a 10 Hz cutoff, the optimal Ω_{gw} is 6.5×10^{-10} at 5 W and it worsens (albeit not significantly) up to 6.9×10^{-10} at 200 W. Also, reducing the low-frequency cutoff improves the sensitivity. For example, when we use a 125 W laser, a 10 Hz cutoff has a limit of 6.84×10^{-10} while a 20 Hz cutoff has 7.8×10^{-10} .

In addition, another two observations can be made from the high power region of Fig. 6.

- The relation between laser power and the optimal Ω_{gw} limit is log-like. Because of the log-like relation, about fifty percent of the sensitivity increase from 5 W to 200 W lies in the jump between 5 W and 10 W.
- The relation between the low-frequency cutoff and the optimal Ω_{gw} limit is non-linear. The gap between the 20 Hz line and the 15 Hz line in Fig. 6 is much larger than the gap between the 15 Hz line and the 10 Hz line. This reflects the rapid change in the interferometer's sensitivity at low frequencies.

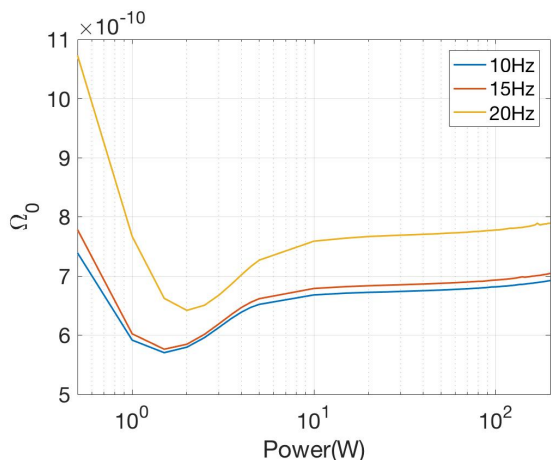


FIG. 6: Plot of the SGWB sensitivity limit versus power and low-frequency cutoff. It can be seen that above ~ 2 W an interferometer with a lower laser power is more sensitive to SGWB, and the sensitivity turns over and becomes worse for powers below ~ 2 W.

In order to look further into how the laser power affects

sensitivity, we compare the noise spectra of some example laser powers in Fig. 7. The noise spectra for 5 W, 50 W, 125 W and 200 W optimal configurations are plotted. One can see that the high frequency minimum shifts to the low frequency region as power decreases, lowering the noise at the low frequency region at the cost of high frequencies. Eventually at 5 W, both dips are below 100 Hz and this contributes to the low-frequency optimization. This explains the improvement of sensitivity when using low laser power.

The reason for the low frequency improvements is the reduction of radiation pressure noise. Laser power is directly related to the radiation pressure noise [19], which dominates the quantum noise at low frequencies [24]. Considering the significance of the low-frequency $h_n(f)$ shown in Eq. 6, we arrive at the point where lower laser power gives lower radiation pressure noise, which in turn leads to the low-frequency improvement shown in Fig. 7 and finally gives better sensitivity limit seen in Fig. 6.

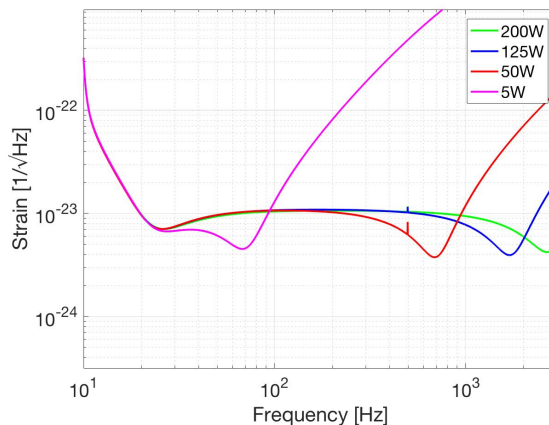


FIG. 7: Dependence of the optimal SGWB noise spectra on laser power. The powers considered are 5 W, 50 W, 125 W and 200 W, and the spectra plotted uses optimal signal recycling configurations. With the increase of laser power, the bottom part of the spectra becomes narrower, and the local minimum on the right shifts to lower frequencies. This low frequency improvement leads to a better sensitivity for the SGWB search.

IV. OPTIMIZING THE SEARCH FOR A COMPACT BINARY PRODUCED SGWB

In Eq. 4, we write a general model for $\Omega_{gw}(f)$ with two parameters α and the reference frequency f_{ref} . For all the work above, we assumed a flat SGWB model, $\alpha = 0$, as is given in Eq. 5. Here we explore a model that represents the background produced by compact binary mergers (binary black holes or binary neutron stars) over the history of the universe [14, 15], where $\alpha = 2/3$ is assumed. Certainly there are proposed SGWBs where the frequency dependence is different [2], but we concentrate

on the two models that are most likely to be detected by the advanced detector network in the coming years [15]. We will optimize the signal recycling for a SGWB search with this $\alpha = 2/3$ frequency dependence and compare the results with the flat $\alpha = 0$ model.

A. The $\alpha = 2/3$ model and sensitivity limit

If we use $\alpha = 2/3$ in Eq. 4, we get

$$\Omega_{gw}(f) = \Omega_{2/3} \left(\frac{f}{f_{ref}} \right)^{2/3}. \quad (7)$$

We can represent the detection sensitivity limit with $\Omega_{2/3}$ and, following the same derivations as Eq. 6 [1], we find the sensitivity limit in this case is

$$\Omega_{\alpha} \geq \frac{25\pi c^2}{16\rho_c G} \sqrt{\frac{2}{T}} \left[\int \frac{\gamma^2(\vec{x}_1, \vec{x}_2, f)}{h_n^4(f) f^{6-2\alpha} f_{ref}^{2\alpha}} df \right]^{-1/2}, \quad (8)$$

where $\alpha = 2/3$.

B. The optimization results

Assuming $\alpha = 2/3$, we find the optimal transmission and SRC detuning phase for every laser power usage. The results are shown in the top and middle plots of Fig. 8, which are very similar to the results in Fig. 5. The optimal transmission increases with power at low powers and decreases for high powers. The optimal phase decreases with as the power increase. Therefore, the use of the $\alpha = 2/3$ power law model does not significantly affect the optimal configurations.

The optimal $\Omega_{2/3}$ as a function of laser power is shown in the bottom plot of Fig. 8. The relation is also similar to the flat model in Fig. 6, with $\Omega_{2/3}$ increasing with laser power or low-frequency cutoff above ~ 2 W and decreasing below. The similarity is not surprising considering that in both Eq. 6 and Eq. 8, the low-frequency noise spectrum contributes more than the high frequency spectrum when $\alpha = 2/3$.

C. Comparisons of the $\alpha = 0$ model and $\alpha = 2/3$ models

The work above optimizes the SRM for the SGWB search using both the flat $\alpha = 0$ model and the power law $\alpha = 2/3$ model (see Eq. 4). In this section, we investigate how the flat optimal configurations perform when the power law model is assumed and, similarly, how the power law optimal configurations perform when the flat model is assumed.

For each set of the optimal configurations with the flat model, we compute its $\Omega_{2/3}$ limit given as Eq. 8. Also, for each set of optimal configurations for the power law

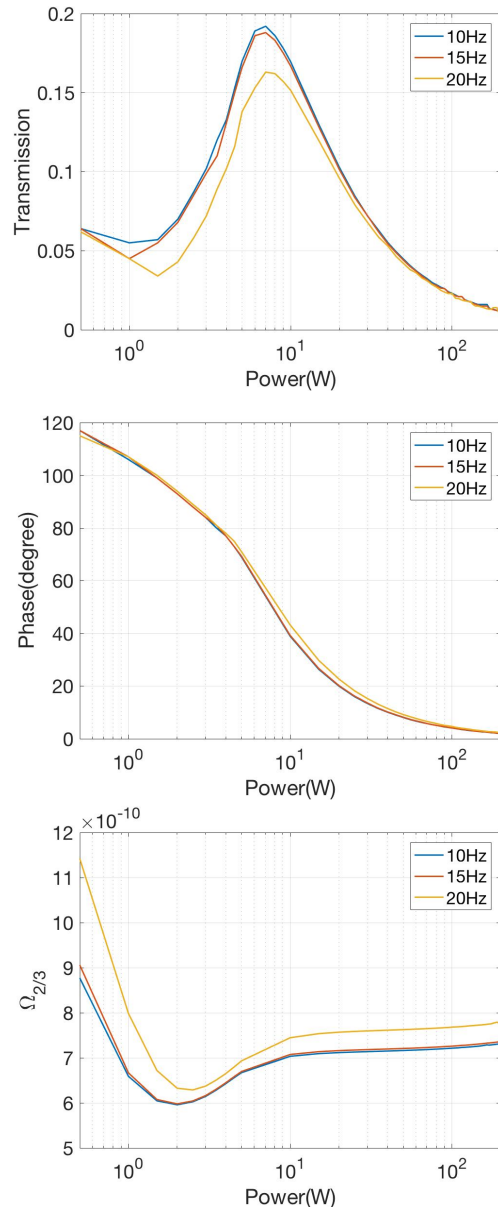


FIG. 8: The optimization of the SGWB search assuming the an $\alpha = 2/3$ model given in Eq. 7. On the top is the SRM transmission and in the middle is the SRC detuning phase. On the bottom is $\Omega_{2/3}$ as is given in Eq. 8. The relations are all similar to the flat model shown in fig. 5.

model, we compute its Ω_0 limit given as Eq. 6. We have comparisons for each frequency cutoff of 10 Hz, 15 Hz and 20 Hz. The comparison plots are shown in Fig. 9.

The first row of Fig. 9 assumes the $\alpha = 0$ model for the SRM configuration. A comparison is made between the derived optimal Ω_0 value for the $\alpha = 0$ model and the resulting $\Omega_{2/3}$ value for the $\alpha = 2/3$ model. The left, middle and right plots assumes 10 Hz, 15 Hz and 20 Hz low-frequency cutoff respectively. The second row

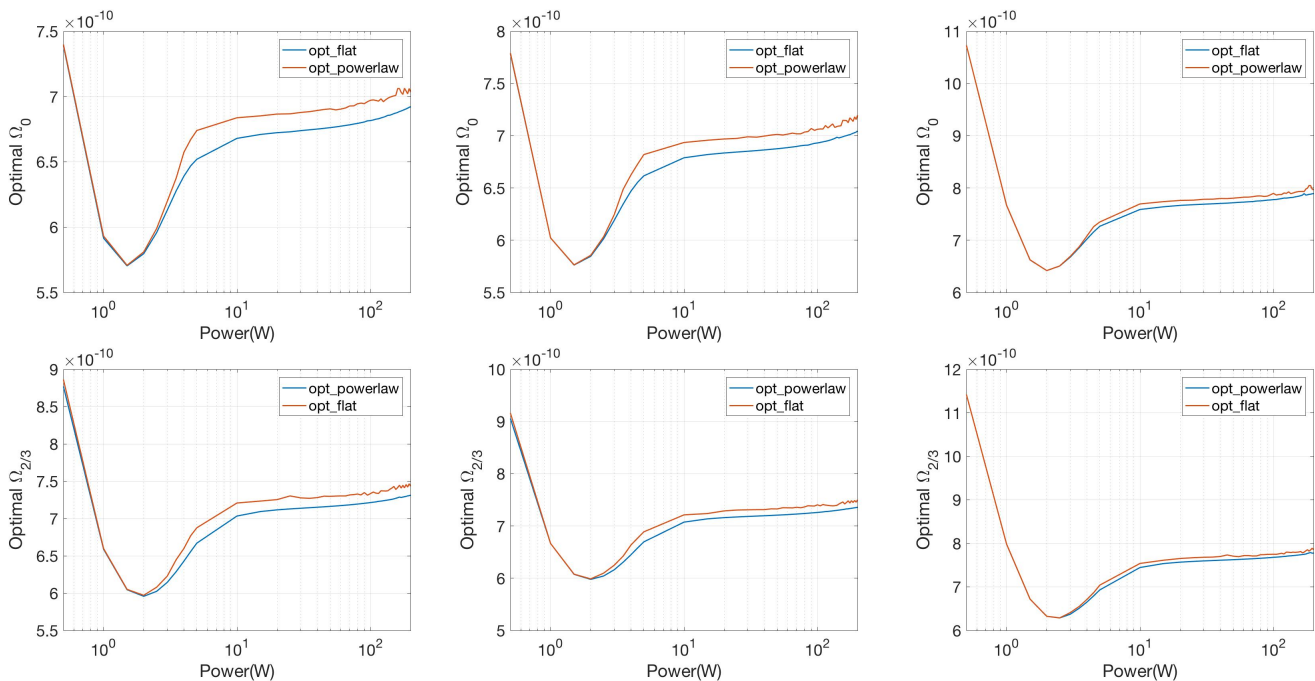


FIG. 9: Comparisons of the sensitivities optimized for the $\alpha = 2/3$ power law and the flat $\alpha = 0$ SGWB models. On the top, left, middle, right are 10 Hz, 15 Hz, 20 Hz comparisons assuming the flat model. Bottom is the same assuming the power law model. Based on the comparisons, it is found that an optimal configuration for one model has a sensitivity close to the optimal sensitivity in another model.

shows the same comparisons assuming $\alpha = 2/3$. In all the plots, the blue lines show the configurations optimized for the flat model and the yellow line shows the configurations optimized for the power law model. It can be seen that the gaps between the lines in Fig. 9 are approximately 10^{-11} . Therefore, the sensitivity difference between a configuration optimized assuming $\alpha = 0$ and another configuration optimized assuming $\alpha = 2/3$ is roughly 10^{-11} . Thus, compared to Ω_α on the order of 10^{-9} and 10^{-10} , a difference of 10^{-11} is not very significant.

V. CONCLUSION

The SRM transmission and SRC detuning phase are optimized for the SGWB search with different laser power usages, low-frequency cutoffs and models for the frequency dependence of Ω_{gw} . For a 125 W laser and a low-frequency cutoff at 10 Hz, the optimal transmission is found to be 1.6% and the optimal phase 3° . The sensitivity for the SGWB search and BNS search for four configurations are compared. It is confirmed that a signal recycled interferometer system is more sensitive for SGWB and BNS searches. Also, the BNS optimized configuration is found to have relatively good sensitivity for both the SGWB search and the BNS search. However, we subsequently found that it is difficult to achieve better sensitivities for both the SGWB and BNS searches with

adjustments to the SRM.

There might be some ways to address the compatibility issue of the BNS search and the SGWB searches, which could lead to potential future studies. First, if we were to use only one mirror, we might be able to fine-adjust the configurations around the regions where the high-sensitivity regions touch in Fig. 4 to get a BNS range over 200 Mpc and a SGWB upper limit around $\Omega < 10^{-9}$. This might require the transmission value be accurate to 0.1% and phase to 0.1° . On the other hand, we might consider replacing the mirrors for different tasks. That would be simple in our studies but could lead to more on-site engineering challenges.

The optimization is then generalized to interferometers with different laser powers and frequency cutoffs. It turns out that using lower laser powers above 2 W results in higher optimal transmission, higher optimal SRC detuning phase and better sensitivity for a SGWB search. Besides, the cutoff frequency does not have a significant effect on the optimal configurations but a lower cutoff gives better sensitivity.

Finally, we consider the SGWB produced by all the compact binary mergers in the history of the universe. This gives us a power law model given in Eq. 7. The $\alpha = 2/3$ power law model does not significantly change the optimization. Actually, configurations optimized for the flat $\alpha = 0$ model have sensitivities that are close to the optimal sensitivities for the $\alpha = 2/3$ power law model. This would mean that an optimized configuration, either

for the flat model or the power law model, would have good sensitivities for both.

In the future, one might envision implementing even more complicated signal recycling systems. The addition of an internal signal recycling mirror between the SRM and the beamsplitter and an optomechanical filter module were recently proposed to achieve a broadband resonance [25]. Besides, different models for a SGWB can also be considered. Gravitational-wave emission from the BNS post-merger remnant is expected to produce a SGWB above 1 kHz [25]. It will be of scientific interest to look further into the optimization of more

complicated signal recycling systems for different models of the SGWB above 1 kHz.

ACKNOWLEDGEMENTS

This work is supported by National Science Foundation (NSF) grant PHY-1505373 to Carleton College. We would also like to thank Peter Fritschel for kindly providing feedback and suggestions during multiple stages of this work. Vuk Mandic and Xingjiang Zhu also provided useful comments.

-
- [1] Bruce Allen and Joseph D. Romano. Detecting a stochastic background of gravitational radiation: Signal processing strategies and sensitivities. *Phys. Rev.*, D59:102001, 1999.
 - [2] B. P. Abbott et al. Upper Limits on the Stochastic Gravitational-Wave Background from Advanced LIGO's First Observing Run. *Phys. Rev. Lett.*, 118:121101, Mar 2017.
 - [3] L. Lentati et al. European Pulsar Timing Array limits on an isotropic stochastic gravitational-wave background. *Monthly Notices of the Royal Astronomical Society*, 453(3):2576–2598, 2015.
 - [4] P. A. R. Ade et al. Planck early results. I. The Planck mission. *A&A*, 536:A1, 2011.
 - [5] Paul D. Lasky, Chiara M. F. Mingarelli, Tristan L. Smith, John T. Giblin, Eric Thrane, Daniel J. Reardon, Robert Caldwell, Matthew Bailes, N. D. Ramesh Bhat, Sarah Burke-Spolaor, Shi Dai, James Dempsey, George Hobbs, Matthew Kerr, Yuri Levin, Richard N. Manchester, Stefan Osłowski, Vikram Ravi, Pablo A. Rosado, Ryan M. Shannon, Renée Spiewak, Willem van Straten, Lawrence Toomey, Jingbo Wang, Linqing Wen, Xiaopeng You, and Xingjiang Zhu. Gravitational-Wave Cosmology across 29 Decades in Frequency. *Phys. Rev. X*, 6:011035, Mar 2016.
 - [6] B. P. et al. Abbott. Observation of Gravitational Waves from a Binary Black Hole Merger. *Phys. Rev. Lett.*, 116:061102, Feb 2016.
 - [7] BP Abbott, R Abbott, TD Abbott, MR Abernathy, F Acernese, K Ackley, C Adams, T Adams, P Addesso, RX Adhikari, et al. GW151226: Observation of gravitational waves from a 22-solar-mass binary black hole coalescence. *Physical Review Letters*, 116(24):241103, 2016.
 - [8] BP Abbott, R Abbott, TD Abbott, MR Abernathy, F Acernese, K Ackley, C Adams, T Adams, P Addesso, RX Adhikari, et al. Binary black hole mergers in the first advanced LIGO observing run. *Physical Review X*, 6(4):041015, 2016.
 - [9] Benjamin P Abbott, R Abbott, TD Abbott, F Acernese, K Ackley, C Adams, T Adams, P Addesso, RX Adhikari, VB Adya, et al. GW170104: Observation of a 50-Solar-Mass Binary Black Hole Coalescence at Redshift 0.2. *arXiv preprint arXiv:1706.01812*, 2017.
 - [10] B. P. Abbott et al. Gw170608: Observation of a 19 solar-mass binary black hole coalescence. *The Astrophysical Journal Letters*, 851(2):L35, 2017.
 - [11] Benjamin P Abbott, R Abbott, TD Abbott, F Acernese, K Ackley, C Adams, T Adams, P Addesso, RX Adhikari, VB Adya, et al. GW170814: A three-detector observation of gravitational waves from a binary black hole coalescence. *Physical Review Letters*, 119(14):141101, 2017.
 - [12] Benjamin P Abbott, R Abbott, TD Abbott, F Acernese, K Ackley, C Adams, T Adams, P Addesso, RX Adhikari, VB Adya, et al. GW170817: observation of gravitational waves from a binary neutron star inspiral. *Physical Review Letters*, 119(16):161101, 2017.
 - [13] F Acernese et al. Advanced virgo: a second-generation interferometric gravitational wave detector. *Classical and Quantum Gravity*, 32(2):024001, 2015.
 - [14] B. P. Abbott et al. GW150914: Implications for the stochastic gravitational wave background from binary black holes. *Phys. Rev. Lett.*, 116(13):131102, 2016.
 - [15] Benjamin P. Abbott et al. GW170817: Implications for the Stochastic Gravitational-Wave Background from Compact Binary Coalescences. *arXiv preprint arXiv:1710.05837*, 2017.
 - [16] J. Aasi et al. Advanced LIGO. *Class. Quant. Grav.*, 32:074001, 2015.
 - [17] Brian J. Meers. Recycling in laser-interferometric gravitational-wave detectors. *Phys. Rev. D*, 38:2317–2326, Oct 1988.
 - [18] Nelson Christensen. *On measuring the stochastic gravitational radiation background with laser interferometric antennas*. PhD thesis, Massachusetts Institute of Technology., 1990.
 - [19] A. Buonanno and Y. Chen. Quantum noise in second generation, signal-recycled laser interferometric gravitational-wave detectors. *Phys. Rev. D*, 64(4):042006, August 2001.
 - [20] Robert D. Guenther. *Modern Optics*. John Wiley & Sons, 1990.
 - [21] Frank L Pedrotti, Leno S Pedrotti, and Leno M Pedrotti. *Introduction to optics*. Pearson Education, Inc, 2007.
 - [22] Nelson Christensen. Measuring the stochastic gravitational-radiation background with laser-interferometric antennas. *Phys. Rev. D*, 46:5250–5266, Dec 1992.
 - [23] LIGO. Gravitational Wave Interferometer Noise Calculator. <https://awiki.ligo-wa.caltech.edu/aLIGO/GWINC>, 2017.

- [24] Thomas Randall Corbitt. *Quantum Noise and Radiation Pressure Effects in High Power Optical Interferometers*. PhD thesis, Massachusetts Institute of Technology., 2001. <http://dspace.mit.edu/handle/1721.1/45452>.
- [25] Haixing Miao, Huan Yang, and Denis Martynov. Towards the design of gravitational-wave detectors for probing neutron-star physics. *arXiv preprint arXiv:1712.07345*, 2017.